

# Origin of sawtooth domain walls in ferroelectrics

J. Zhang,<sup>1</sup> Y.-J. Wang,<sup>2</sup> J. Liu,<sup>3</sup> J. Xu,<sup>1</sup> D. Wang,<sup>1,\*</sup> L. Wang,<sup>4</sup> X.-L. Ma,<sup>2</sup> C.-L. Jia,<sup>1,5</sup> and L. Bellaïche<sup>6</sup>

<sup>1</sup>*School of Microelectronics & State Key Laboratory for Mechanical Behavior of Materials, Xi'an Jiaotong University, Xi'an 710049, China*

<sup>2</sup>*Shenyang National Laboratory for Materials Science, Institute of Metal Research, Chinese Academy of Sciences, Wenhua Road 72, 110016 Shenyang, China*

<sup>3</sup>*State Key Laboratory for Mechanical Behavior of Materials, School of Materials Science and Engineering, Xi'an Jiaotong University, Xi'an 710049, China*

<sup>4</sup>*Electronic Materials Research Laboratory, School of the Electronic and Information Engineering, Xi'an Jiaotong University, Xi'an 710049, China*

<sup>5</sup>*Ernst Ruska Center for Microscopy and Spectroscopy with Electrons, Research Center Jülich, D-52425 Jülich, Germany*

<sup>6</sup>*Department of Physics and Institute for Nanoscience and Engineering, University of Arkansas Fayetteville, Arkansas 72701, USA*

(Dated: May 29, 2019)

Domains and domain walls are among the key factors that determine the performance of ferroelectric materials. In recent years, a unique type of domain walls, i.e., the sawtooth shaped domain walls, has been observed in BiFeO<sub>3</sub> and PbTiO<sub>3</sub>. Here, we build a minimal model to reveal the origin of these sawtooth shaped domain walls. Incorporating this model into Monte-Carlo simulations shows that (i) the competition between the long-range Coulomb interaction (due to bound charges) and short-range interaction (due to opposite dipoles) is responsible for the formation of these peculiar domain walls and (ii) their relative strength is critical in determining the periodicity of these sawtooth shaped domain walls. Necessary conditions to form such domain walls are also discussed.

Domains, which are typical regions with aligned magnetic moments or electric dipoles, can largely influence phase transitions and physical properties of magnetic or ferroelectric materials. For ferroelectrics, many attentions have been paid to investigate domains' characteristics and properties [1–5]. When changing from the paraelectric to the ferroelectric phase, the symmetry of equivalent dipole directions is broken, giving rise to regions with different polarization directions while each region has a preferred polarization direction. Ferroelectric domain walls have received extensive attention due to various novel phenomena, including stable patterns on the nanometer scale. Domains have been carefully analyzed to reveal the correlation between the micro/nanoscale structure and the properties of the materials [6–9], often through high resolution X-ray diffraction technique [10, 11]. For instance, polarization switching is a critical link between domains and material performance [12–17]. In bulk ferroelectrics, the domain structure, closely related to phase structure, was thoroughly discussed along with domain size and morphology. On an even smaller scale, polar nanoregions as a special type of domains have also been discussed [18–23].

Due to the competition between the electrostatic energy (aligned dipoles usually have smaller electrostatic energy) and the domain wall energy (the extra energy necessary to have domains), domains can have very different morphologies, such as rhombohedral, orthorhombic, and tetragonal domains [24]. However, it was still quite surprising when sawtooth shaped 180° domain walls were observed in multiferroic BiFeO<sub>3</sub> (BFO) (see Fig. 4(a) of Ref. [25]), which has a spontaneous polarization along the pseudocubic  $\langle 111 \rangle_c$  direction (that can be as large as 90–95  $\mu\text{C}/\text{cm}^2$  [26]) and a high Curie temperature ( $T_C = 820^\circ\text{C}$ ) [27–29]. Note that the BiFeO<sub>3</sub> sample of Ref. [25] was cut along  $\langle \bar{1}\bar{1}0 \rangle$  and  $\langle 1\bar{1}0 \rangle$  while extending 55 nm vertically when high resolution trans-

mission electron microscopy (HRTEM) images were taken. More recently, Zou *et al.* [30] also observed serrated 180° domain walls in PbTiO<sub>3</sub> (PTO) thin films prepared by pulsed laser deposition. This PTO thin film was 100 nm thick and epitaxially grown on a (100)-oriented single crystal SrTiO<sub>3</sub> substrate (see Figs. 2 and 4 of Ref. [30]). These observations indicate that sawtooth-shaped domain wall constitute a general phenomenon in ferroelectrics, not limited to multiferroics or magnetic materials [31, 32]. Since such domain walls involve head-to-head dipoles, the bound charge on the walls can be quite large (for BFO, the bound charge is estimated to be  $1.64|e_0|$ , where  $e_0$  is the electron charge [33]), which can strongly affect the conductivity of the material by attracting free charge carriers, making them good candidates for domain wall electronics [34–36]. Recent research also show that negative capacitance is also closely related to dipole patterns and domain structures [37, 38]. In this work, we explore possible causes of this unique phenomenon of sawtooth-shaped domain walls, finding that the long-range Coulomb between bound charges and the short-range interaction between opposite dipole pairs are adequate to reproduce such peculiar domain walls.

As a matter of fact, in order to understand the sawtooth domain walls, we propose a minimal model with just short-range interaction between opposite dipoles and long-range Coulomb interaction due to bound charges arising from the head-to-head dipoles, and following a similar approach as the effective Hamiltonian [39–44] to simulate 2D and 3D ferroelectric materials. We assume that (i) electric dipoles of opposite directions already exist in the system, and (ii) a boundary exists between the two groups of opposite dipoles (see Fig. 1). As bound charges accumulate on the boundary, their positions can be used as dynamic variables in simulations while the number of bound charges is fixed, which determines both

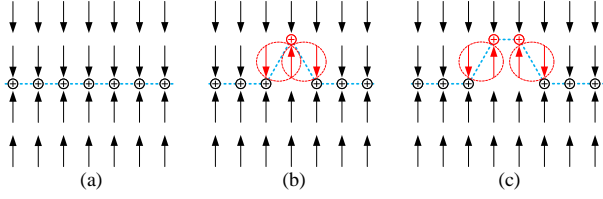


Figure 1. Schematic drawing of dipoles and bound charges. (a) The black arrows represent dipoles, while the blue line depicts the  $180^\circ$  domain wall. The symbol “ $\oplus$ ” between dipoles represents bound charges formed by head-to-head dipoles. (b) When a dipole is reversed, the domain wall and the position of one bound charge change accordingly, and two pairs of opposite electric dipole pairs are generated at the left and right sides of the reversed dipole. (c) Another configuration can also involve two pairs of opposite dipoles.

the Coulomb energy and the short-range interaction as Fig. 1 shows. Therefore, the total energy for the system is given by:

$$E^{\text{tot}} = E^{\text{cc}}(\{\mathbf{r}_i\}) + E^{\text{short}}(\{\mathbf{r}_i\}) \quad (1)$$

where  $\mathbf{r}_i$  is the position of the  $i$ th bound charge.  $E^{\text{short}}$  is the short-range energy when neighboring ions have relative shifts [39]. For the 2D case shown in Fig. 1, the short-range interaction on the domain wall can be expressed as  $E^{\text{short}} = JN$ , where  $J > 0$  is the additional energy associated with opposite neighboring dipoles and  $N$  (depending on  $\{\mathbf{r}_i\}$ ) is the number of opposite dipole pairs.  $E^{\text{cc}} = \frac{1}{2} \sum_{i,j} Z^2 / |\mathbf{r}_i - \mathbf{r}_j|$  is the long-range charge-charge Coulomb energy, where  $Z$  is the bound charge and the energy unit is Hartree. Since the sawtooth domain wall induces bound charges and opposite dipole pairs,  $E^{\text{tot}}$  can also be regarded as the formation energy of the domain wall. For simplicity, we use the energy of Fig. 1(a) as the reference energy  $E_0$ , implicitly subtracting  $E_0$  from  $E^{\text{tot}}$  hereafter.

Using the total energy of Eq. (1), Monte-Carlo (MC) simulations are employed to find the equilibrium domain wall morphology. During the simulation, the position of the bound charges ( $\mathbf{r}_i$ ) are tracked and changed to minimize the free energy. In each MC simulation at 300 K, we perform 320,000 sweeps of all the  $\mathbf{r}_i$ . We will first show the simulation results and then discuss how the parameters ( $J$  and  $Z$ ) can affect the morphology.

For the 2D case, we use a  $60 \times 60$  supercell to mimic a planar sample. The bound charge is chosen as  $Z = 1.16|e_0|$ , which is an approximate estimation from the  $R3c$  phase  $\text{BiFeO}_3$  [33], while the short-range interaction parameter is taken to be  $J = 0.042$  Hartree (1 Hartree = 27.2 eV) [45] We note the parameter  $J$  can be estimated by comparing  $E^{\text{tot}}$  here [46] to the formation energy of an inclined charged domain wall obtained from first-principles calculations [47]. The effect of these parameters on the sawtooth domain walls will be further discussed later. Figure 2 displays a typical 2D simulation result, in which the sawtooth domain walls can be clearly seen. The domain walls have an approximate periodicity of

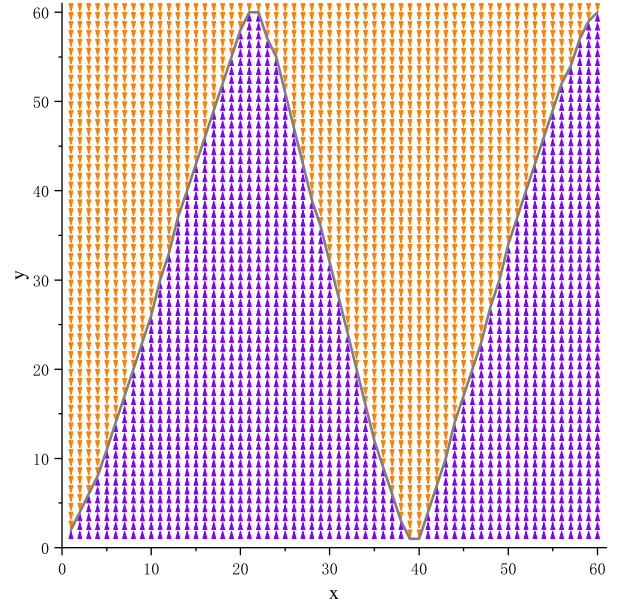


Figure 2. Sawtooth shaped domain wall in a  $60 \times 60$  2D lattice.

40 lattices and can steadily exist for 200,000 MC sweeps.

For the 3D case, we use the Ewald method [48], which naturally models the periodic boundary conditions of the supercell, to accelerate the evaluation of the Coulomb energy. The short-range interaction is treated similarly as in 2D, except that four nearest neighbors need to be considered instead of two. We note that, considering experimental situation (e.g., PTO on STO where ferroelectric regions are separated by non-ferroelectric ones), we do not assume bound charge exist on the top-bottom boundary

Using a  $40 \times 10 \times 40$  supercell, we carry out 320,000 sweeps of MC simulation at 300 K, and the resulting domain wall is shown in Fig. 3(a). Figure 3(b) shows the cross section at  $y = 8$  where a triangular sawtooth domain wall can be clearly seen. To compare to experimental HRTEM images, we have also projected the dipoles along the  $y$  direction, averaging along each column, which results in Fig. 3(c). This figure not only demonstrates the sawtooth domain walls, but can also explain the smaller dipoles separating the two domains as observed in experiment [see Fig. 5(a) of Ref. [25]].

As we have seen, this model, which involves only Coulomb and short-range interactions, is adequate to reproduce the sawtooth domain walls. With this model, it is also possible to reveal and understand how  $Z$  and  $J$  can affect the domain wall morphology. To simplify the analysis, we use the 2D case as an example and only consider triangular sawtooth domain walls with different periodicities (see Fig. 4). The length of the domain wall can be formally defined as (in unit of  $a_0$ )  $l = \sum_i \sqrt{(x_{i+1} - x_i)^2 + (y_{i+1} - y_i)^2}$ , where  $\mathbf{r}_i = a_0(x_i, y_i)$  is the position of the  $i$ th charge and  $a_0$  is the lattice constant. As shown in Fig. 4,  $x_{i+1} - x_i = 1$ , therefore  $l = \sum_i \sqrt{1 + (y_{i+1} - y_i)^2}$ . Because the bound charge can only shift

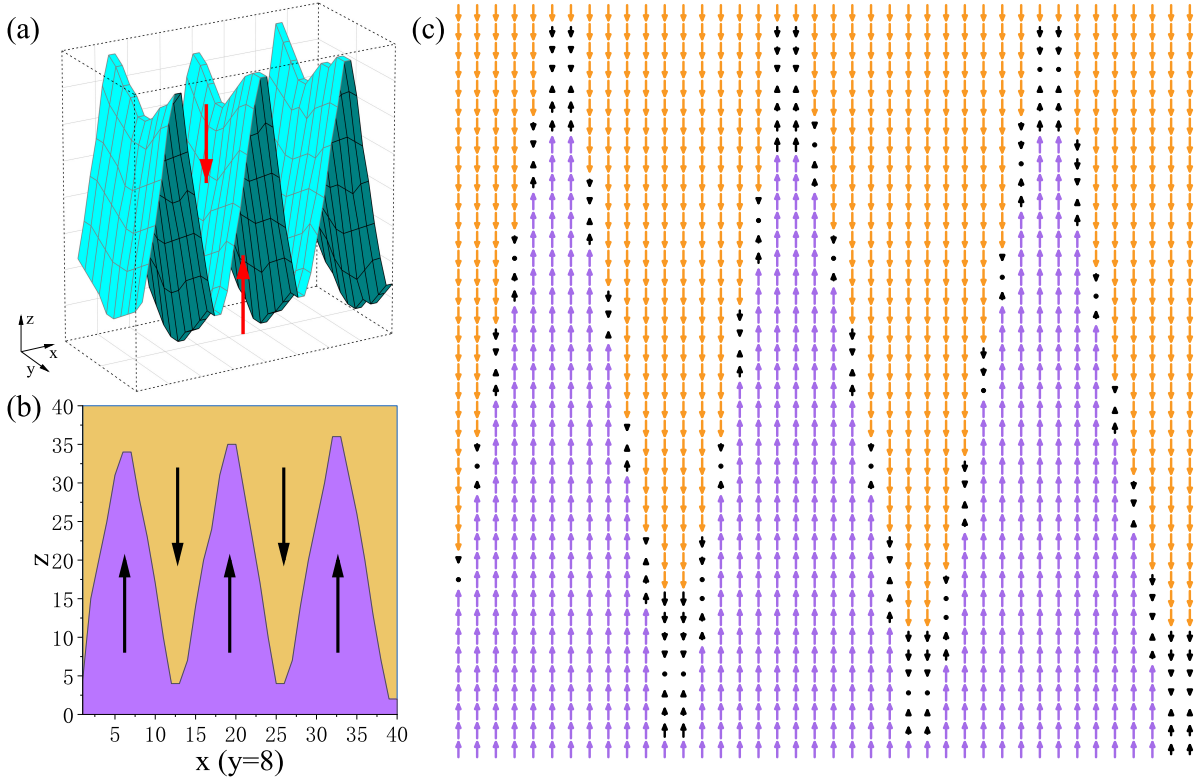


Figure 3. Sawtooth shaped domain wall in the 3D using a  $40 \times 40 \times 10$  supercell. (a) It contains a series of conical depressions and bulges; (b) The cross section at  $y = 8$  shows a jagged domain wall; (c) The projection of the dipoles on the  $x$ - $z$  plane shows reduced dipoles (black arrows) due to the average of dipoles over different  $y$  sections.

in the up and down directions, the  $l$  can be further simplified to its  $y$  component as

$$l = \sum_i |y_{i+1} - y_i|, \quad (2)$$

which can unambiguously determine the triangular domain wall. One advantage of this definition is that the short-range energy is directly proportional to  $l$  (see Fig. 5a), i.e.  $E^{\text{short}} = Jl$ . The Coulomb energy also depends on  $l$  as  $E^{\text{cc}} = E^{\text{cc}}(l) - E_0^{\text{cc}}$  where  $E_0^{\text{cc}} = Z^2\gamma/a_0$  (in unit of Hartree) and  $\gamma$  is a constant calculated according to the charge positions shown in Fig. 4(a).

As  $l$  increases, the domain wall becomes sharper and the periodicity becomes smaller [see Fig. 4(b)]. Given a domain wall length, we can numerically calculate its constituent energies, which are shown as symbols in Fig. 5. It can be seen that the Coulomb energy and the short-range interaction energy show opposite trends with the length of domain wall. The short-range interaction increases with  $l$ , since larger  $l$  means more opposite dipole pairs. The Coulomb energy decreases with  $l$  due to the increase of bound charge distance.

To proceed further, we propose to use  $E^{\text{cc}} = \frac{Z^2\gamma}{a_0} \left( \frac{1+bl^2}{1+al^2} - 1 \right)$  to describe how the Coulomb energy changes with  $l$ , where  $\gamma = 220.8$  for a  $60 \times 60$  simulation

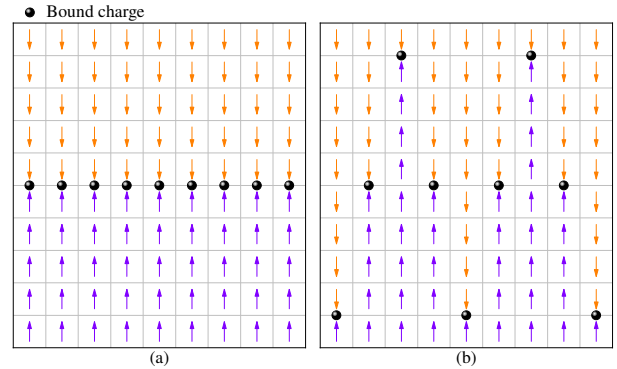


Figure 4. Schematic diagram of the domain wall shape changing with its length. (a) In this case, the length of the domain wall is zero, it has the minimal short-range interaction and maximal Coulomb interaction. (b) As the length becomes larger, the domain wall appears inclined and sharper. The Coulomb interaction decreases while the short-range interaction increases.

box. As a matter of fact, this expression can be used to fit the numerically computed Coulomb energy in Fig. 5, giving  $a = 1.99 \times 10^{-4}$  and  $b = 7.18 \times 10^{-5}$ . The total energy is then given by

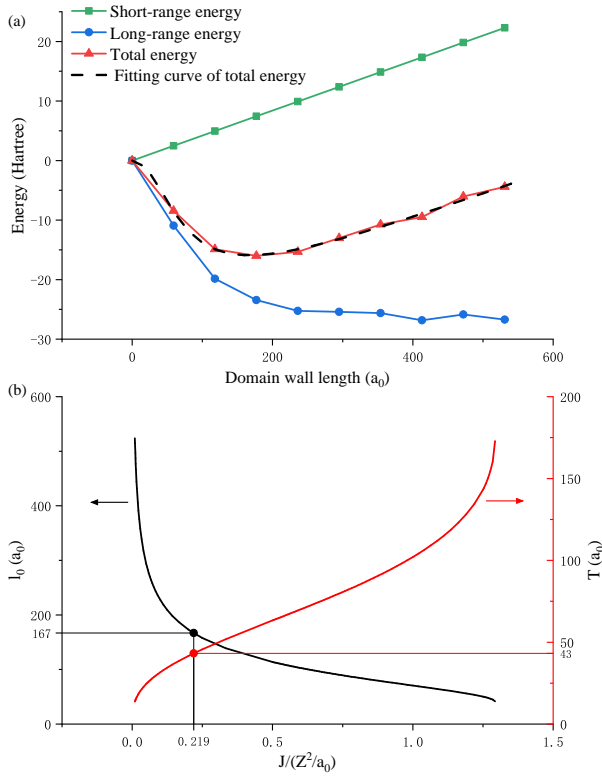


Figure 5. (a) The constituent energies versus the length of the domain wall. The short-range interaction increases linearly, while the Coulomb interaction decreases (symbols are from numerical computations); (b) The stabilized domain wall length ( $l_0$ , black line) and periodicity ( $T$ , red line) versus  $J/(Z^2/a_0)$ .

$$E^{\text{tot}} = Jl + \frac{Z^2\gamma}{a_0} \left( \frac{1+bl^2}{1+al^2} - 1 \right), \quad (3)$$

The variation of the total energy with  $l$  is also shown in Fig. 5(a). The equilibrium domain wall length  $l_0$  can be found by minimizing the total energy with respect to  $l$ , and its dependence on  $J/(Z^2/a_0)$  is shown in Fig. 5(b). This result indicates that the parameter  $\alpha \equiv J/(Z^2/a_0)$  is crucial for determining the domain morphology and larger  $\alpha$  tends to bind the bound charges closer to each other.

In the simulations that generate Figs. 2 and 3,  $\alpha = 0.22$  is used. The resulting domain wall length and sawtooth period are consistent with the theoretical estimation. In numerically obtaining  $l_0$  for Fig. 5(b), we find that when  $\alpha > 1.29$ , no solution can be found for  $l_0$ , which is consistent with our numerical findings (not shown here) that arbitrarily chosen  $J$  and  $Z$  cannot support the existence of such domain walls.

It shall be noted that the precondition for the above analysis is that triangular domain walls already exist. The constraint of  $\alpha < 1.29$  can be understood by estimating the two energies of the configuration shown in Fig. 4(b). Assuming that two neighboring bound charges are shifted by  $y$  vertically, the short-range interaction is  $NJy$  ( $N = 60$  for the

$60 \times 60$  simulation box), while the Coulomb energy pertaining to this configuration is the horizontal line of bound charges [Fig. 4(a)] tilted by an angle of  $\alpha$  ( $\tan \alpha = y$ ), giving the energy of  $(Z^2\gamma/a_0) \left( 1/\sqrt{1+y^2} - 1 \right)$ . Since the Coulomb energy and the short-range interaction energy shall balance each other (not that one overwhelms the other) and reduce the total energy, therefore  $NJy + Z^2\gamma/a_0 \left( 1/\sqrt{1+y^2} - 1 \right) < 0$  is necessary, resulting in  $\alpha < \gamma \left( 1 - 1/\sqrt{1+y^2} \right) / (Ny) \leq 1.10$  for  $N = 60$ , where the maximum is reached when  $y = 1.27$ . Since the Coulomb energy in the triangular case shall be larger than this value as the bound charges are closer, the final value of  $\alpha$  shall be smaller than 1.10.

In fact, a more stringent constraint can be obtained with Fig. 4(a) as the initial configuration and consider only one bound charge (the first one from the left) is shifted upward by  $y$ , which satisfies  $Jy + (Z^2/a_0) \sum_{i=1}^N \left( 1/\sqrt{n^2+y^2} - 1/n \right) < 0$  or  $\alpha < \sum_{i=1}^N \left( 1/n - 1/\sqrt{n^2+y^2} \right) / y \leq 0.42$  where the maximum is reached when  $y = 1.7$ . This result further constrains the parameters that can form sawtooth domain walls, indicating that there is an upper bound for  $\alpha$  to make the sawtooth domain walls possible. This constraint, which is necessary to form sawtooth domain walls, is also verified using MC simulation. For materials with large dielectric constant, still smaller  $J$  is required since the Coulomb energy is now proportional to  $Z^2/\epsilon_r a_0$ , where  $\epsilon_r > 1$  is the relative permittivity.

In addition to the constraint on  $\alpha$ , it was pointed out that  $180^\circ$  domain occurs when no (or very small) epitaxial strain are applied from the substrate, while  $90^\circ$  or other domain patterns are expected with larger values [30, 49, 50]. Our result here reveals the reason behind such observations: strain (especially local strain) or defects, which can couple with the dipoles, will effectively increase  $J$ , eventually making the sawtooth domain walls impossible to form.

In summary, we have built a minimal model to reveal the origin of the sawtooth shaped domain walls observed in ferroelectric materials. Our model based MC simulations show that the competition between the long-range Coulomb energy from bound charges and the short-range interaction energy are responsible for the formation of these peculiar domain walls. Further analysis also shows that the combined parameter  $J/(Z^2/a_0)$  is critical in determining the periodicity of the sawtooth shaped domain walls and its value has to satisfy certain conditions for this unique type of domain walls to appear in ferroelectrics.

This work is financially supported by the National Natural Science Foundation of China (Grant No. 11574246, U1537210, and 51671194), National Basic Research Program of China (Grant No. 2015CB654903, 2014CB921002), and the Key Research Program of Frontier Sciences CAS (QYZDJ-SSW-JSC010). D.W. also thanks the support from China Scholarship Council (201706285020). L.B. acknowledges ARO Grant No. W911NF-16-1-0227.

\* dawei.wang@xjtu.edu.cn

- [1] W. J. Merz, *Domain formation and domain wall motions in ferroelectric BaTiO<sub>3</sub> single crystals*, Phys. Rev. **95**, 690 (1954).
- [2] S. Wada, K. Yako, H. Kakemoto, T. Tsurumi, and T. Kiguchi, *Enhanced piezoelectric properties of barium titanate single crystals with different engineered-domain sizes*, J. Appl. Phys. **98**, 014109 (2005).
- [3] K. Yako, H. Kakemoto, T. Tsurumi, and S. Wada, *Domain size dependence of d<sub>33</sub> piezoelectric properties for bariumtitanate single crystals with engineered domain configurations*, Mater. Sci. Eng., B **120**, 181 (2005).
- [4] H. J. Lee, S. J. Zhang, J. Luo, F. Li, and T. R. Shrout, *Thickness-Dependent Properties of Relaxor-PbTiO<sub>3</sub> Ferroelectrics for Ultrasonic Transducers*, Adv. Funct. Mater. **20**, 3154 (2010).
- [5] D. B. Lin, S. J. Zhang, Z. R. Li, F. Li, Z. Xu, S. Wada, T. R. Shrout, *Domain size engineering in tetragonal Pb(In<sub>1/2</sub>Nb<sub>1/2</sub>)O<sub>3</sub>-Pb(Mg<sub>1/3</sub>Nb<sub>2/3</sub>)O<sub>3</sub>-PbTiO<sub>3</sub> crystals*, J. Appl. Phys. **110**, 084110 (2011).
- [6] E. A. Little, *Dynamic behavior of domain walls in barium titanate*, Phys. Rev. **98**, 978 (1955).
- [7] C. T. Nelson, P. Gao, J. R. Jokisaari, C. Heikes, C. Adamo, A. Melville, S. H. Baek, C. M. Folkman, B. Winchester, Y. Gu, Y. Liu, K. Zhang, E. Wang, J. Li, L.-Q. Chen, C.-B. Eom, D. G. Schlom and X. Pan, *Domain dynamics during ferroelectric switching*, Science **334**, 968 (2011).
- [8] M. Dawber, K. M. Rabe, J. F. Scott, *Physics of thin-film ferroelectric oxides*, Rev. Mod. Phys. **77**, 1083 (2005).
- [9] P. Gao, J. Britson, J. R. Jokisaari, C. T. Nelson, S. H. Baek, Y. Wang, C. B. Eom, L. Chen and X. Panet, *Atomic-scale mechanisms of ferroelastic domain-wall-mediated ferroelectric switching*, Nat. Commun. **4**, 2791 (2013).
- [10] Y. M. Jin, Y. U. Wang, A. G. Khachatryan, and J. F. Li, D. Viehland, *Conformal Miniaturization of Domains with Low Domain-Wall Energy: Monoclinic Ferroelectric States near the Morphotropic Phase Boundaries*, Phys. Rev. Lett. **91**, 197601 (2003).
- [11] W. S. Chang, L. C. Lim, P. Yang, C. M. Hsieh, and C. S. Tu, *Rhombohedral and tetragonal nanotwin domains and thermally induced phase transformations in PZN-8%PT single crystals*, J. Phys.: Condens. Matter **20**, 445218 (2008).
- [12] A. Roelofs, N. A. Pertsev, R. Waser, F. Schlaphof, L. M. Eng, C. Ganpule, V. Nagarajan, and R. Ramesh, *Depolarizing-field-mediated 180 degrees switching in ferroelectric thin films with 90 degrees domains*, Appl. Phys. Lett. **80**, 1424 (2001).
- [13] D. J. Jung, M. Dawber, J. F. Scott, L. J. Sinnamon, and J. M. Gregg, *Switching dynamics in ferroelectric thin films: An experimental survey*, Integrat. Ferroelectr. **48**, 59 (2002).
- [14] R. Gysel, I. Stolichnov, N. Setter, and M. Pavius, *Ferroelectric film switching via oblique domain growth observed by cross-sectional nanoscale imaging*, Appl. Phys. Lett. **89**, 082906 (2006).
- [15] S. Prosandeev, B. Xu, and L. Bellaiche, *Polarization switching in the PbMg<sub>1/3</sub>Nb<sub>2/3</sub>O<sub>3</sub> relaxor ferroelectric: An atomistic effective Hamiltonian study*, Phys. Rev. B **98**, 024105 (2018).
- [16] S. Boyn, J. Grollier, G. Lecerf, B. Xu, N. Locatelli, S. Fusil, S. Girod, C. Carrétéro, K. Garcia, S. Xavier, J. Tomas, L. Bellaiche, M. Bibes, A. Barthélémy, S. Saighi and V. Garcia, *Learning through ferroelectric domain dynamics in solid-state synapses*, Nat. Commun. **8**, 14736 (2017).
- [17] B. Xu, V. Garcia, S. Fusil, M. Bibes, and L. Bellaiche, *Intrinsic polarization switching mechanisms in BiFeO<sub>3</sub>*, Phys. Rev. B **95**, 104104 (2017).
- [18] H. Wang, J. Zhu, N. Lu, A. A. Bokov, Z.-G. Ye, X. W. Zhang, *Hierarchical Micro/Nanoscale Domain Structure in Mc Phase of (1-x)Pb(Mg<sub>1/3</sub>Nb<sub>2/3</sub>)O<sub>3</sub>-xPbTiO<sub>3</sub> Single Crystal*, Appl. Phys. Lett. **89**, 042908 (2006).
- [19] F. Bai, J. Li, D. Viehland, *Domain hierarchy in annealed (001)-oriented Pb(Mg<sub>1/3</sub>Nb<sub>2/3</sub>)O<sub>3</sub>-xPbTiO<sub>3</sub> single crystals*, Appl. Phys. Lett. **85**, 2313 (2004).
- [20] G. Xu, J. Wen, C. Stock, and P. M. Gehring, *Phase instability induced by polar nanoregions in a relaxor ferroelectric system*, Nat. Mater. **7**, 562 (2008).
- [21] M. F. Wong, K. Zeng, *Nanoscale domains and preferred cracking planes in Pb(Zn<sub>1/3</sub>Nb<sub>2/3</sub>)O<sub>3</sub>-(6-7)% PbTiO<sub>3</sub> single crystals studied by piezoresponse force microscopy and fractography*, J. Appl. Phys. **107**, 124104 (2010).
- [22] A. Al-Barakaty, S. Prosandeev, D. Wang, B. Dkhil and L. Bellaiche, *Finite-temperature properties of the relaxor PbMg<sub>1/3</sub>Nb<sub>2/3</sub>O<sub>3</sub> from atomistic simulations*, Phys. Rev. B **91**, 214117 (2015).
- [23] A. R. Akbarzadeh, S. Prosandeev, E. J. Walter, A. Al-Barakaty and L. Bellaiche, *Finite-Temperature Properties of Ba(Zr,Ti)O<sub>3</sub> Relaxors From First Principles*, Phys. Rev. Lett. **108**, 257601 (2012).
- [24] Y. L. Li, S. Y. Hu, and L. Q. Chen, *Ferroelectric domain morphologies of (001) Pb(Zr<sub>1-x</sub>, Ti<sub>x</sub>)O<sub>3</sub> epitaxial thin films*, J. Appl. Phys. **97**, 034112 (2005).
- [25] C.-L. Jia, L. Jin, D. Wang, S. B. Mi, M. Alexe, D. Hesse, H. Reichlova, X. Marti, L. Bellaiche, and K. W. Urbana, *Nanodomains and nanometer-scale disorder in multiferroic bismuth ferrite single crystals*, Acta Mater. **82**, 356 (2015).
- [26] Y.-H. Chu, L. W. Martin, M. B. Holcomb, and R. Ramesh, *Controlling magnetism with multiferroics*, Mater. Today, **10**, 16 (2007).
- [27] J. Wang, J. B. Neaton, H. Zheng, V. Nagarajan, S. B. Ogale, B. Liu, D. Viehland, V. Vaithyanathan, D. G. Schlom, U. V. Waghmare, N. A. Spaldin, K. M. Rabe, M. Wuttig, and R. Ramesh, *Epitaxial BiFeO<sub>3</sub> Multiferroic Thin Film Heterostructures*, Science **299**, 1719 (2003).
- [28] J. R. Teague, R. Gerson and W. J. James, *Dielectric hysteresis in single crystal BiFeO<sub>3</sub>*, Solid State Commun. **8**, 1073 (1970).
- [29] D. Wang, J. Weerasinghe, and L. Bellaiche, *Atomistic Molecular Dynamic Simulations of Multiferroics*, Phys. Rev. Lett **109**, 067203 (2012).
- [30] M. Zou, Y. Tang, Y. Feng, Y. Zhu, X. Ma, *Ferroelectric thin films in the 180° charged domain wall of the scale structure features*, J. Chin. Electr. Microsc. Soc. **37**, 468 (2018).
- [31] N. Curland and D. E. Speljotić, *Transition region in recorded magnetization patterns*, J. Appl. Phys. **41**, 1099 (1970).
- [32] K. Moon, J. Cho, C. Kim, J. Yoon, D. Kim, K. Song, B. Chun, D. Kim, and C. Hwang, *Triangular and sawtooth magnetic domains in measuring the Dzyaloshinskii-Moriya interaction*, Phys. Rev. Appl. **10**, 064014 (2018).
- [33] The estimated value of 1.64 |e<sub>0</sub>| is obtained using ρ<sup>bound</sup> = -∇ · P, assuming |P| = 95 μC/cm<sup>2</sup> and BiFeO<sub>3</sub>'s lattice constant. The value (1.16 |e<sub>0</sub>|) used in the MC simulations are obtained by considering the parameters used in the effective Hamiltonian for BiFeO<sub>3</sub> [29] and the local mode value numerically obtained at 300 K.
- [34] J. Seidel, L. W. Martin, Q. He, Q. Zhan, Y.-H. Chu, A. Rother, M. E. Hawkrige, P. Maksymovych, P. Yu, M. Gajek, N. Balke, S. V. Kalinin, S. Gemming, F. Wang, G. Catalan, J. F. Scott, N. A. Spaldin, J. Orenstein, and R. Ramesh, *Conduction at domain walls in oxide multiferroics*, Nat. Mater. **8**, 229-234 (2009).
- [35] L. J. McGilly, C. S. Sandu, L. Feigl, D. Damjanovic, and N.

- Setter, *Nanoscale Defect Engineering and the Resulting Effects on Domain Wall Dynamics in Ferroelectric Thin Films*, Adv. Funct. Mater. **27**, 1605196 (2017).
- [36] P. Sharma, D. Sando, Q. Zhang, X. Cheng, S. Prosandeev, R. Bulanadi, S. Prokhorenko, L. Bellaiche, L. Q. Chen, V. Nagarajan and J. Seidel, *Conformational Domain Wall Switch*, Adv. Funct. Mater. 1807523 (2019). DOI:10.1002/adfm.201807523
- [37] T. Sluka, P. Mokry, and N. Setter, *Static negative capacitance of a ferroelectric nano-domain nucleus*, Appl. Phys. Lett. **111**, 152902 (2017).
- [38] I. Luk'yanchuk, Y. Tikhonov, A. Sené, A. Razumnaya, and V.M. Vinokur, *Harnessing ferroelectric domains for negative capacitance*, Commun. Phys. **2**, 22 (2019).
- [39] W. Zhong, D. Vanderbilt, and K. M. Rabe, *First-principles theory of ferroelectric phase transitions for perovskites: The case of BaTiO<sub>3</sub>*, Phys. Rev. B **52**, 6301 (1995).
- [40] S. Prosandeev, D. Wang, A. R. Akbarzadeh and L. Bellaiche, *First-principles-based effective Hamiltonian simulations of bulks and films made of lead-free Ba(Zr,Ti)O<sub>3</sub> relaxor ferroelectrics*, J. Phys.: Condens. Matter **27**, 223202 (2015).
- [41] V. Bhall, R. Kuma, C. Tripath, and D. Sing, *Mechanical and thermal properties of praseodymium monopnictides: an ultrasonic study*, Int. J. Mod Phys B **27**, 1330016 (2013).
- [42] H. Ye, D. Wang, Z. Jiang, S. Cheng, and X. Wei, *Ferroelectric phase transition of perovskite SnTiO<sub>3</sub> based on the first principles*, Acta Phys. Sinica **65**, 237101 (2016).
- [43] D. Wang, J. Hlinka, A. A. Bokov, Z. G. Ye, P. Ondrejovic, J. Petzelt, and L. Bellaiche, *Fano resonance and dipolar relaxation in lead-free relaxors*, Nat. Commun. **5**, 5100 (2014).
- [44] D. Wang, A. A. Bokov, Z. G. Ye, J. Hlinka, and L. Bellaiche, *Subterahertz dielectric relaxation in lead-free Ba(Zr,Ti)O<sub>3</sub> relaxor ferroelectrics*, Nat. Commun. **7**, 11014 (2016).
- [45] The value of  $J$  used in this work is obtained using BiFeO<sub>3</sub>'s the effective Hamiltonian parameter [29] representing the nearest-neighbor short-range interaction of different dipole configuration (see Fig. 1 of Ref. [39]).
- [46] For comparison to first-principles calculations, the calculation of the Coulomb energy  $E^{\text{cc}}$  needs to adopt realistic dielectric constant of the given material.
- [47] Y. X. Jiang, Y. J. Wang, D. Chen, Y. L. Zhu, and X. L. Ma, *First-principles study of charged steps on 180° domain walls in ferroelectric PbTiO<sub>3</sub>*, J. App. Phys. **122**, 054101 (2017).
- [48] D. Wang, J. Liu, J. Zhang, S. Raza, X. Chen, and C.-L. Jia, *Ewald summation for ferroelectric perovskites with charges and dipoles*, Comp. Mater. Sci. **162**, 314 (2019).
- [49] Y. L. Li, S. Y. Hu, Z. K. Liu, L. Q. Chen, *Effect of substrate constraint on the stability and evolution of ferroelectric domain structures in thin films*, Acta Mater. **50**, 395 (2002).
- [50] Y. Wang, Y. Zhu, and X. L. Ma, *Chiral phase transition at 180° domain walls in ferroelectric PbTiO<sub>3</sub> driven by epitaxial compressive strains*, J. Appl. Phys. **122**, 134104 (2017).